Available online at www.sciencedirect.com
ScienceDirect
Journal of Solid State Chemistry 180 (2007) 1636–1647
JOURNAL OF SOLID STATE CHEMISTRY
www.elsevier.com/locate/jssc

Synthesis and characterization of sulfate and dodecylbenzenesulfonate intercalated zinc–iron layered double hydroxides by one-step coprecipitation route

Hui Zhang[a,*], Xing Wen[a], Yingxia Wang[b]

[a]State Key Laboratory of Chemical Resource Engineering, Beijing University of Chemical Technology, Box 98, Beijing 100029, China
[b]State Key Laboratory of Rare Earth Materials Chemistry and Applications, College of Chemistry and Molecular Engineering, Peking University, Beijing 100871, China

Received 14 November 2006; received in revised form 5 March 2007; accepted 12 March 2007
Available online 21 March 2007

Abstract

Inorganic sulfate- and organic dodecylbenzenesulfonate (DBS)-intercalated zinc–iron layered double hydroxides (LDHs) materials were prepared by one-step coprecipitation method from a mixed salt solutions containing Zn(II), Fe(II) and Fe(III) salts. The as-prepared samples have been characterized by X-ray powder diffraction (XRD), Fourier-transform infrared spectroscopy (FT-IR), low-temperature nitrogen adsorption, scanning electron microscopy (SEM), inductively coupled plasma emission spectroscopy (ICP), and Mössbauer spectroscopy (MS). The XRD analyses demonstrate the typical LDH-like layered structural characteristics of both products. The room temperature MS results reveal the characteristics of both the Fe(II) and Fe(III) species for SO_4^{2-}-containing product, while only the Fe(III) characteristic for DBS-containing one. The combination characterization results and Rietveld analysis illustrate that the SO_4^{2-}-containing product possesses the Green Rust two (GR2)-like crystal structure with an approximate chemical composition of $[Zn_{0.435} \cdot Fe^{II}_{0.094} \cdot Fe^{III}_{0.470} \cdot (OH)_2] \cdot (SO_4^{2-})_{0.235} \cdot 1.0H_2O$, while the DBS-containing one exhibits the common LDH compound-like structure. The contact angle measurement indicates the evident hydrophobic properties of DBS-containing nanocomposite, compared with SO_4^{2-}-containing product, due to the modification of the internal and external surface of LDHs by the organic hydrophobic chain of DBS.

Keywords: Layered double hydroxides; ZnFe(II)Fe(III) GR2(SO_4^{2-}); Dodecylbenzene-sulfonate-ZnFe-LDHs; Coprecipitation; Rietveld analysis

1. Introduction

Typical Fe^{II}–Fe^{III}-containing layered double hydroxides (LDH), also known as Green Rust (GR) compounds, have the normalized chemical formula $[Fe^{II}_{1-x}Fe^{III}_x(OH)_2]^{x+}[(x/n)A^{n-} \cdot (mx/n)H_2O]^{x-}$, where positively charged hydroxide layers $[Fe^{II}_{1-x}Fe^{III}_x(OH)_2]^{x+}$ alternate with negatively charged interlayers of anions A^{n-} and with m water molecules per anion [1–4]. Two types of X-ray diffraction (XRD) patterns exist; Green Rust one (GR1) incorporates planar anions and Green Rust two (GR2) incorporates 3-dimensional anions [5–7]. Particularly, the structure and stability of Fe^{II}–Fe^{III} GR compound incorporated with 3-dimensional sulfate anions, belong to the GR2 type, have been widely investigated by Genin et al. [6,7]. This type of LDH compounds are chemically reactive due to the presence of iron(II) species. For instance, the synthetic GR, $[Fe^{II}_4Fe^{III}_2(OH)_2]^{2+} \cdot [SO_4^{2-} \cdot mH_2O]^{2-}$, generally by aerial oxidation of Fe(II) hydroxide suspensions, was demonstrated to be able to reduce in abiotic conditions polluting species such as nitrate, Cr(VI) and Se(VI) ions [2,6,8–10]. Nevertheless, a few papers reported the partial substitution of Fe^{2+} by other divalent cation such as Mg^{2+}, Ni^{2+}, and Co^{2+}, for instance, a promising method for preparing high quality spinel compounds from a series of $M^{II}Fe^{II}Fe^{III}$-LDHs (M = Mg, Ni, Co) layered precursors developed by Li et al. [11] and an intermediate

*Corresponding author. Fax: +86 10 6442 5385.
E-mail address: huizhang67@gst21.com (H. Zhang).

0022-4596/$ - see front matter © 2007 Elsevier Inc. All rights reserved.
doi:10.1016/j.jssc.2007.03.016

structure between the GR and the pyroaurite-type compounds for Fe(II)Mg(II)Fe(III)-CO_3-LDH revealed by Refait et al. [12]. The introduction of the second bivalent cation in GR compounds may lead to obvious structure and property changes and consequently holds promise in application aspects of the resultant LDHs compounds.

However, to the best of our knowledge, it is rare to focus on the synthesis and structure studies on incorporation of Zn^{2+} into Green Rust compounds and intercalation of organic anions, such as anionic surfactant, into Zn–Fe-containing LDHs compounds. Upon the fact that the hydrophilic nature of the LDHs intercalated with small inorganic anions can be modified into hydrophobic one with long alkyl chain-containing anionic surfactants substituting the interlayer inorganic anions [13–19], the organic-incorporating resultants are promising adsorbents for the removal of hydrophobic organic contaminants from wasting water.

In present work, we synthesize a novel $ZnFe^{II}Fe^{III}$ hydroxylsulfate GR compounds and a novel organic surfactant dodecylbenzenesulfonate (DBS)-intercalated zinc–iron LDHs by simple coprecipitation method for the first time. The structure and physico-chemical properties of as-prepared precipitates were characterized by powder X-ray diffraction (XRD), low-temperature N_2-adsorption, Fourier transform infrared (FT-IR), Mössbauer spectroscopy (MS), scanning electron microscopy (SEM), thermogravimetric and differential thermal analysis (TG-DTA), and contact angle determinations. The layer structure and chemical composition of sulfate-containing product have been proposed on the basis of Rietveld analysis and combinational spectroscopy characterizations including inductively coupled plasma (ICP) emission spectroscopy data.

2. Materials and methods

2.1. Materials

All the chemicals used in this work were of analytical grade and used without further purification. Decarbonated and deionized water was used and N_2 was bubbled throughout the preparation process to minimize soluble CO_2 concentration.

2.2. Synthesis

Sulfate intercalated LDH was synthesized by adding dropwise NaOH aqueous solution (1 mol/L) into a 100 mL mixed aqueous solution of $ZnSO_4 \cdot 7H_2O$ (0.0192 mol), $FeSO_4 \cdot 7H_2O$ (0.01 mol) and $Fe_2(SO_4)_3 \cdot 7H_2O$ (0.01 mol) ($Fe^{2+}/Fe^{3+} = 1/2$) under vigorous stirring and N_2 atmosphere at room temperature till the final pH $\simeq$ 7.0. The resulting mixtures were aged at 40 °C for 15 h, followed by filtration and washing several times and then dried in vacuum. The precipitate is denoted SO_4-LDHs, and it is gray-green in color.

DBS-intercalated LDH was prepared by adding NaOH aqueous solution (1 mol/L) into a 100 mL mixed aqueous solution containing $ZnCl_2$ (0.0192 mol), $FeCl_2 \cdot 4H_2O$ (0.01 mol), $FeCl_3 \cdot 6H_2O$ (0.01 mol) ($Fe^{2+}/Fe^{3+} = 1/1$) and sodium dodecylbenzenesulfonate (0.01 mol) under vigorous stirring and N_2 atmosphere at room temperature till the pH $\simeq$ 7.0. Here iron chloride was used because of the selectivity that LDHs and related compounds exhibit with respect to different anions, implying in particular that divalent anions are always preferred to monovalent ones [13,19]. The resulting mixture was aged at 60 °C for 40 h, followed by filtration and washing several times and then dried in vacuum. The precipitate is denoted DBS-LDHs, and it is brown-yellow in color.

2.3. Characterization techniques

Powder X-ray diffraction (XRD) data were collected at room temperature on a Rigaku D/max-2000 diffractometer with Cu $K\alpha$ radiation and graphite monochromator. Sample SO_4-LDHs was sealed by mylar film for avoiding the degradation of the GR sample, which is sensitive to the air. The measurement was operated at conditions of 40 kV and 100 mA. The scans were taken in steps of 0.02° and the remaining time of each step was 1 s. The data for SO_4-LDHs were over the range of 2θ from 5° to 100°. For DBS-LDHs, the data were collected in two sections—the first section was from 1° to 12° using slits 1/6 (divergence), 1/6 (anti-scattering) and 0.15 (receiving) and the second section was from 4° to 100° using slits 1/2(divergence), 1/2(anti-scattering) and 0.30 (receiving). The data of the first section were normalized according to the intensity ratio of the crossing part in the two sections and combined to the second section to get the wide spectra of 1–100°. The X-ray diffraction data were processed with program TOPAS [20]. The structure model of SO_4-LDHs was taken from GR II(SO_4) [6] and the Rietveld refinement was performed. For DBS-LDHs, only profile fitting over the range of 4–100° was done.

Analysis of metal element and sulfur was performed by using ICP emission spectroscopy on a Shimadzu ICPS-7500 instrument. The amount of Fe(II) was determined by both oxidation–reduction titration method [21] and MS technique. Carbon and hydrogen analyses were carried out using an Elementarvario elemental analysis instrument.

Mössbauer spectra were recorded on an Oxford MS-500 instrument at 298 K. A radiation source of ^{57}Co in an Rh matrix was used. The isomer shifts are reported relative to sodium nitroprusside.

Low-temperature N_2-adsorption measurement for the sample was recorded using a Quantachrome Autosorb-1 system. Samples pretreated by heating at 353 K under vacuum for 2 h was used to determine the surface areas at 77 K using N_2 as the adsorbate and He as the carrier gas. Specific surface area was calculated by the BET equation.

Fourier transform infrared (FT-IR) spectra were recorded on a Brucker Vector 22 spectrophotometer in the

range 400–4000 cm^{-1} with 2 cm^{-1} resolution. The standard KBr disk method (1 mg of sample in 100 mg of KBr) was used.

The transmission electron micrograph (TEM) was recorded on a HITACHI-800 transmission electron microscope (200 kV). SEM photomicrographs were obtained using a Cambridge S-250 MK3 scanning electron microscope.

Contact angle was measured through the Sessile Drop method using JC2000A contact angle/interface tensile measurer (made in Shanghai). Deionized water drops were used in the measurement, and three measurements were obtained for each sample.

Thermogravimetric analyses (TG) were performed on a locally made PCT-IA at heating rate of 10 °C min^{-1} in airflow.

3. Results and discussion

3.1. Crystal structure, morphology, and surface property

The X-ray powder diffraction patterns of SO_4-LDHs and DBS-LDHs are depicted in Fig. 1(a) and (b), which illustrate the well-organized layered structure of the prepared compounds, respectively, and the basal spacing and lattice parameters are summarized in Table 1.

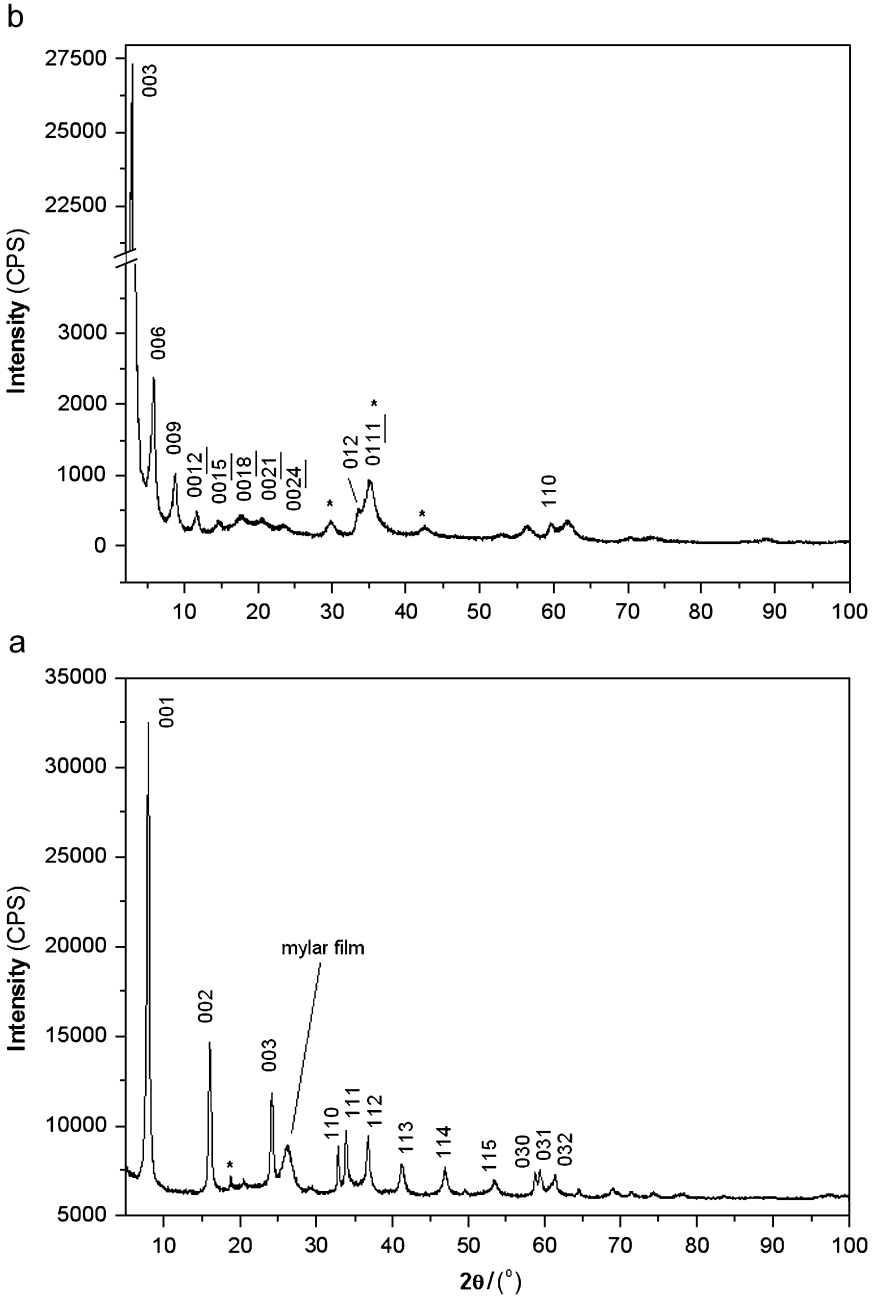

Fig. 1. X-ray powder diffraction patterns of SO_4-LDHs (a) and DBS-LDHs (b).

Table 1
Indexing of XRD patterns of SO_4-LDHs and DBS-LDHs

d_{hkl}[1]	d_{001}/nm	d_{002}/nm	d_{003}/nm	d_{110}/nm	Lattice parameter a/nm	Lattice parameter c/nm
SO_4-LDHs	1.1039	0.552	0.368	0.2722	0.5444_3	1.1039_6
GR2[2]	1.1011	0.548	0.365	0.2762	0.5552_4	1.1011_6
d_{hkl}[3]	d_{003}/nm	d_{006}/nm	d_{009}/nm	d_{110}/nm	Lattice parameter a/nm	Lattice parameter c/nm
DBS-LDHs	3.036	1.518	1.012	0.1549	0.3098	9.109

[1]Originally indexed by Bernal et al. (1959) on a hexagonal cell.
[2]Data from Simon et al. (2003) for GR2(SO_4^{2-}).
[3]Indices based on a hexagonal cell.

The kinds of interlamellar anion strongly influence the interlayer anionic disposition of Fe(II)–Fe(III)-containing compounds of LDHs [1,2,6,12]. As expected, all main lines found in XRD pattern for SO_4-LDHs (Fig. 1(a)) can be assigned to typical of GR(SO_4^{2-}) compound, and the d-spacings are identical to those found by Bernal et al. [22] and Gehin et al. [6,7]. As commonly recognized in the case of GR(SO_4^{2-}) [1,6,7,22], the diffraction data of the prepared SO_4-LDHs are indexed to a hexagonal lattice with parameters $a = 0.5444$ nm and $c = 1.104$ nm (see Table 1) from the d_{hkl} distances observed in the XRD patterns. It should also be noted that the peak at about 2θ 26.2° is due to the use of Mylar film, and the line marked with ∗ in Fig. 1(a) are also due to the GR(SO_4^{2-}) compounds [1,6,22].

The TEM images of SO_4-LDHs shown in Fig. 2(a) and (b) obviously show the thin, approximately hexagonal, plate-like crystals, as commonly observed for typical inorganic anionic intercalated LDH compounds [19], with diameter between 160 and 360 nm. The SEM image (Fig. 2(c)) further demonstrates the approximately hexagonal platy crystallites of SO_4-LDHs with sharp particle edge and similar particle size. The BET measurement shows the specific surface area of 45 m^2/g for SO_4-LDHs, as in the case of most inorganic anions-intercalated LDHs compounds [19].

However, quite differently, all main lines found in the XRD pattern of DBS-LDHs (Fig. 1(b)) are typical of organo-LDHs composite [13], and the d-spacings are similar to those found for DBS intercalated Cu–Al–Fe LDHs [23] and Zn–Cr LDHs [24]. The sharp and intense (003) reflection and a series clear modulation of high-order reflections demonstrate a well-crystallized DBS-intercalated LDHs compound. The basal spacing d_{003} of 3.036 nm is quite larger than that of SO_4-LDHs (Fig. 1(a)), indicating the greatly expanded interlayer spacing due to intercalation of the larger organic DBS anions between the LDH layers. As in the case of DBS-intercalated Zn–Cr LDHs [24], the diffraction data of the DBS-LDHs can be indexed to a hexagonal lattice with parameters $a = 0.3098$ nm and $c = 9.109$ nm from the d_{hkl} distances observed in the XRD pattern. It should be also noted that several weak but clearly identifiable peaks at 2θ 30–65° (∗ in Fig. 1(b)) were carefully assigned to zinc ferrite phase (JCPDS 79–1150).

The TEM (Fig. 2(d) and (e)) and SEM (Fig. 2(f)) images of DBS-LDHs indicate that the DBS-LDHs particle edge is not as sharp as SO_4-LDHs, though the ill-shaped thin plate-like crystals with diameter between 200 and 400 nm are observed. In fact, the DBS-LDHs particles are agglomerated and interconnected with each other as compact and non-porous stacking morphology, and the surfaces are more diffuse, suggesting that there might be some DBS draped over the external surface of the intercalate particles, as observed previously by other authors [17]. The BET measurement shows the very small specific surface area of 1.28 $m^2\,g^{-1}$, consistent with above observation.

The FT-IR spectra of SO_4-LDHs and DBS-LDHs shown in Fig. 3 provide the host–guest interaction information of the LDHs intercalates. The common IR features of the LDH structure can be found for both intercalates with an intense broadband centered at 3443 cm^{-1} due to the OH stretch of hydroxide layers and interlayer water molecules [19,24–26] and a band at 1628 cm^{-1} due to the bending mode of the interlayer structure water [19]. It should be noted that above both bands related to interlayer water molecules of SO_4-LDHs are relatively narrower and stronger than those of DBS-LDHs, suggesting the higher interlayer order of water molecules in the former than in the latter. It is well known that IR spectroscopy is very sensitive to the presence of carbonate anions in LDHs (ν_3 at 1370 cm^{-1}) and the very weak band here enables us to assume that the prepared samples are carbonate free. In particular, the strong band $\nu_3(SO_4^{2-})$ for the synthesized SO_4-LDHs (Fig. 3(a)) is split into two peaks, at 1196 and 1109 cm^{-1}, implying a lowering of site symmetry from Td as in the case of SO_4-containing LDHs compounds [27]. The strong band at 613 cm^{-1} is ascribed to the ν_4, and the weak band at 985 cm^{-1} to the ν_1, whose observation is because the intercalation of SO_4^{2-} between the LDHs layers results in activation of the IR inactive ν_1 [25]. The ν_2 mode is not observed as a separate band due to strong overlap with other lattice vibrations. These data are in accordance with the previously reported unsuitable geometry of 3-dimensional anion SO_4^{2-} anions for the common three-layer repeat stackings of LDHs compound [6,28,29]. Strong hydrogen bond between water molecules and layer hydroxyl groups and interlayer sulfate anions are involved, in addition to the obvious electrostatic

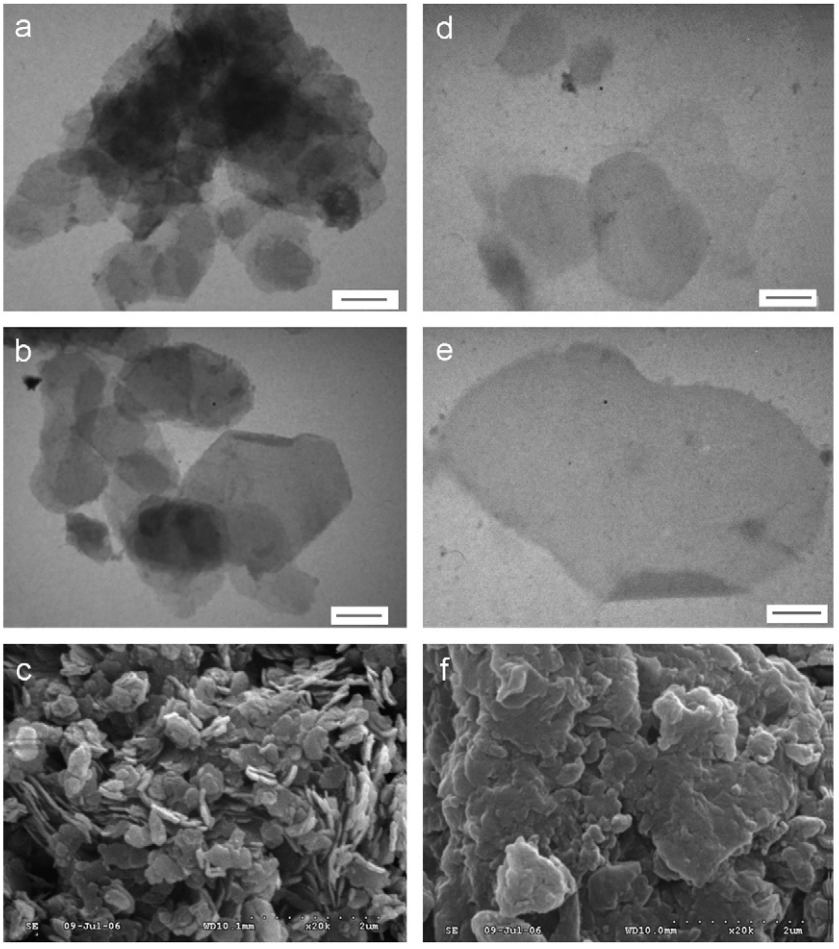

Fig. 2. Electron microscope images for SO_4-LDHs (a–c) and DBS-LDHs (d–f). (a), (b), (d) and (e) represent TEM images with bar scale of 200, 100, 200, 100 nm, respectively. (c) and (f) represent SEM images.

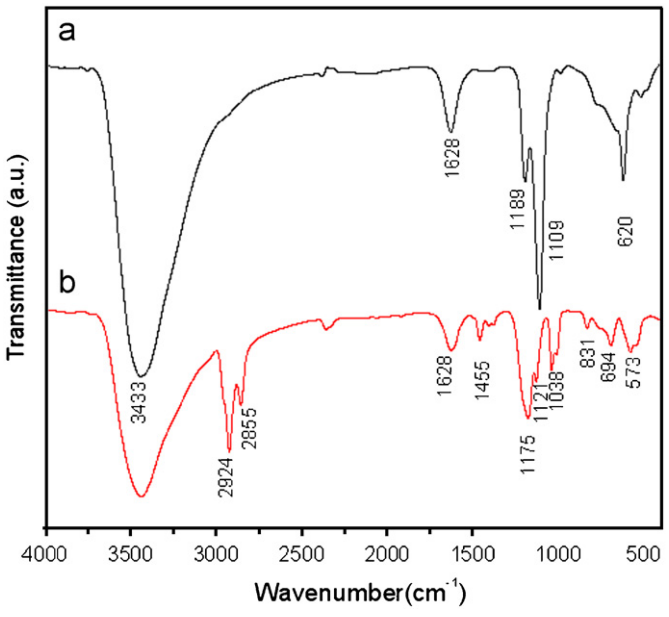

Fig. 3. FT-IR spectra of LDHs (a) SO_4-LDHs, (b) DBS-LDHs and (c) DBS.

attractions between $ZnFe^{II}Fe^{III}$-OH brucite-like layer and the interlayer sulfate anion.

As for DBS-LDHs (Fig. 3(b)), the positions and relative intensities of the bands due to typical C–H stretch (ν_{as} (CH_3) at 2957 cm^{-1}, ν_{as} (CH_2) at 2924 cm^{-1} and ν_s (CH_2) at 2853 cm^{-1}), C–H aromatic in-plane bend (1127 and 1010 cm^{-1}) and out-of-plane bend (831 cm^{-1}), and C–C aromatic stretch (1604, 1502 and 1410 cm^{-1}), closely resemble those for SDBS and the literature values [26,30]. However, the four bands associated with aromatic sulfonate anions, including ν_{as} (S = O) at 1175 cm^{-1} and ν_s (S = O) at 1038 cm^{-1}, and CH_3 symmetrical bending (sharp) at 1365 cm^{-1} and CH_2 scissoring (sharp) at 1456 cm^{-1}, which overlapped with CH_3 asymmetrical-bending (weak shoulder), are obviously shifted to lower frequencies compared with those for SDBS upon intercalation [25]. These information further illustrate the formation of hydrogen bond of benzenesulfonate with the OH group of the layers as well as with the interlayer water via the path S = O……H–O–*M* (*M* present Fe or Zn) in addition to the electrostatic attraction and the possible hydrophobic interactions between the interlayer

DBS anions [14]. In addition, the bands at ca. 542 and 580 cm^{-1} are attributed to the O–*M*–O, *M*–O–*M* and *M*–OH lattice vibrations [19,26].

Contact angle measurements indicate that the inorganic-containing LDHs SO_4-LDHs with strong hydrophilic surface property revealed by the contact angle of 0° for water (Fig. 4(a)) similar to previously reported for CO_3-LDHs [14]. While for DBS-LDHs composite, the contact angle for water is 104° (Fig. 4(b)), which is quite larger than that for pure SDBS (~30°), indicating considerable hydrophobic property upon the intercalation of DBS anions with organic hydrophobic chain between the layers, in good agreement with literature reported [31,32]. Therefore, certain agglomerates or curvature occur due to the hydrophobic modification of LDHs surface by DBS anions, and this affords to its less sharp morphology as previous SEM photo and literature observed [17,31,32].

3.2. Chemical composition, Rietveld analysis, and host–guest interaction

The elemental analysis of dried SO_4-LDHs shows the contents of Zn, Fe and S (in wt%) as 19.88%, 22.46% and 7.3%, respectively. The presence of small amount of Na (0.67%) can be neglected. Taking into account the presence of iron species, especially Fe(II) cation, Mössbauer spectra were recorded. Hyperfine parameters *D*1, *D*3 and *D*4 obtained from computer fitting with Lorentzian-shape lines are given in Table 2. The Mössbauer spectrum of SO_4-LDHs (Fig. 5(a)) displays three doublets *D*1, *D*3 and *D*4. According to the values of isomer shift (δ) and quadrupole splitting (Δ) in Table 2, only one hyperfine parameter *D*1 with $\Delta = 2.425\,mm\,s^{-1}$ and $\delta = 1.007\,mm\,s^{-1}$ corresponds to high spin Fe^{2+} ions in octahedral sites, being consistent with the unique Fe^{2+} characteristic for GR mineral holding SO_4^{2-} as the intercalated anion [6,7,12]. *D*3 and *D*4 with $\Delta = 0.916$ and $0.508\,mm\,s^{-1}$ and $\delta = 0.175$ and $1.180\,mm\,s^{-1}$ correspond to high spin Fe^{3+} ions in octahedral sites [3,12]. Here, the existence of a second Fe^{3+} doublet *D*4 is unusual, since such a doublet does not appear on the spectra of Fe^{2+}–Fe^{3+} hydroxysalts [6,7]. Therefore, it can be attributed to the presence of Zn^{2+} ions as next nearest neighbors. The abundance ratio [Fe^{2+}]/[Fe^{3+}] is found equal to ca. 0.21 by computing the ratio of the doublet intensities $D1/(D3+D4)$, which is lower than the initial input value of 1/2, suggesting that the input Fe^{2+} species are partially oxidized into Fe^{3+} during the synthesis process, though the N_2 atmosphere is employed, consistent with the metastable characteristics of GR-type LDHs compounds [1,6]. Fortunately, the chemical analysis for Fe(II) cation (3.6 wt%) is in good agreement with the Mössbauer spectra data. Combining the TG results for water content (in Section 3.3) and ICP data of S, an approximately derived chemical formula is $[Zn_{0.435}\,Fe^{II}_{0.094}\,Fe^{III}_{0.470}\,(OH)_2]\cdot(SO_4^{2-})_{0.235}\cdot 1.0H_2O$, where the Fe^{3+}/S molar ratio is 2.0, $(Zn+Fe^{II})/Fe^{III}$ molar ratio is 1.13, and the calculated Zn, Fe and S contents of 20.9%, 23.5% and 5.6% are in good agreement with the experimental dada.

Considering the high similarity of the diffraction patterns between the prepared SO_4-LDHs and GR2(SO_4^{2-}) [6], we take the structure model of GR2(SO_4^{2-}) for SO_4-

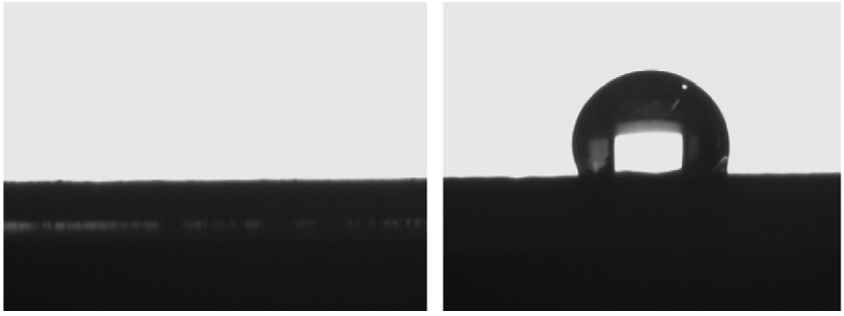

Fig. 4. Effect of intercalation of DBS between the LDH layers. (Left) SO_4-LDHs wetted on contact with water. (Right) Water drop (ca. 12 mm in diameter) fails to wet the DBS-LDHs.

Table 2
Mössbauer parameters measured at room temperature for SO_4-LDHs and DBS-LDHs. δ($mm\,s^{-1}$): isomer shift relative to sodium nitroprusside; Δ($mm\,s^{-1}$): quadrupole splitting; RA (%): relative intensity of peak areas

Samples		Δ ($mm\,s^{-1}$)	Δ ($mm\,s^{-1}$)	FWHM ($mm\,s^{-1}$)	RA(%)
SO_4-LDHs	D1 (Fe^{2+})	1.007	2.425	0.368	17
	D3 (Fe^{3+}(I))	0.175	0.916	0.35	29
	D4 (Fe^{3+}(II))	0.180	0.508	0.315	54
DBS-LDHs	D3 (Fe^{3+}(I))	0.188	0.731	0.447	33
	D4 (Fe^{3+}(II))	0.167	0.448	0.355	67

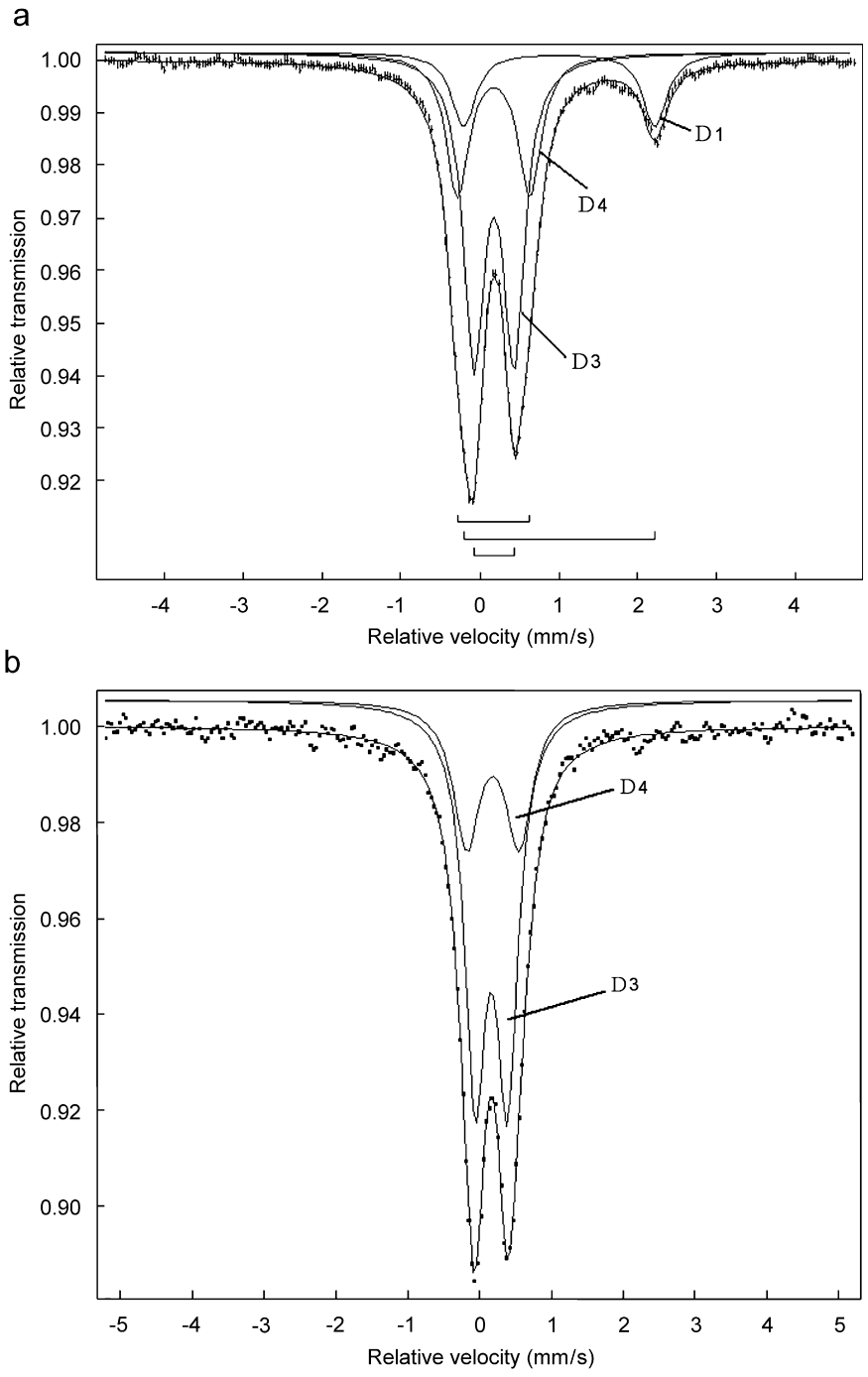

Fig. 5. Mössbauer spectra of (a) SO_4-LDHs and (b) DBS-LDHs.

LDHs structure refinement. In space group *P-31m,* the refinement yielded $a = 0.5444$ nm and $c = 1.104$ nm. The slight shrinking of lattice parameter a, compared with GR2(SO_4^{2-}) (see Table 1), is due to the substitution of smaller Zn^{2+} for Fe^{2+}. According to the derived chemical formula, Fe^{3+} was arranged at 1*a* (0, 0, 0) position, while all Zn^{2+} were in 2*c* position with occupancy 0.645, and the left part of 2*c* positions were taken by Fe^{2+}/Fe^{3+}. The occupancies of Fe^{2+} and Fe^{3+} at 2*c* position were deduced from the chemical formula. Rietveld refinement results are shown in Fig. 6. The positional and thermal parameters for SO_4-LDHs are reported in Table 3. The results confirm that SO_4-LDHs is isostructural with GR2(SO_4^{2-}). The peaks at 2θ 20.8°, 29.3° and 35.2° are from some anonymous scatterings of the sample. The peaks at 2θ 33.0°, 58.7°, 59.6° and 61.4°, corresponding to the indices (110), (030), (031) and (032), reveal the scattering of LDH-layer along (*hk*0), (0*k*0)/(0*kl*). Therefore, the structure of

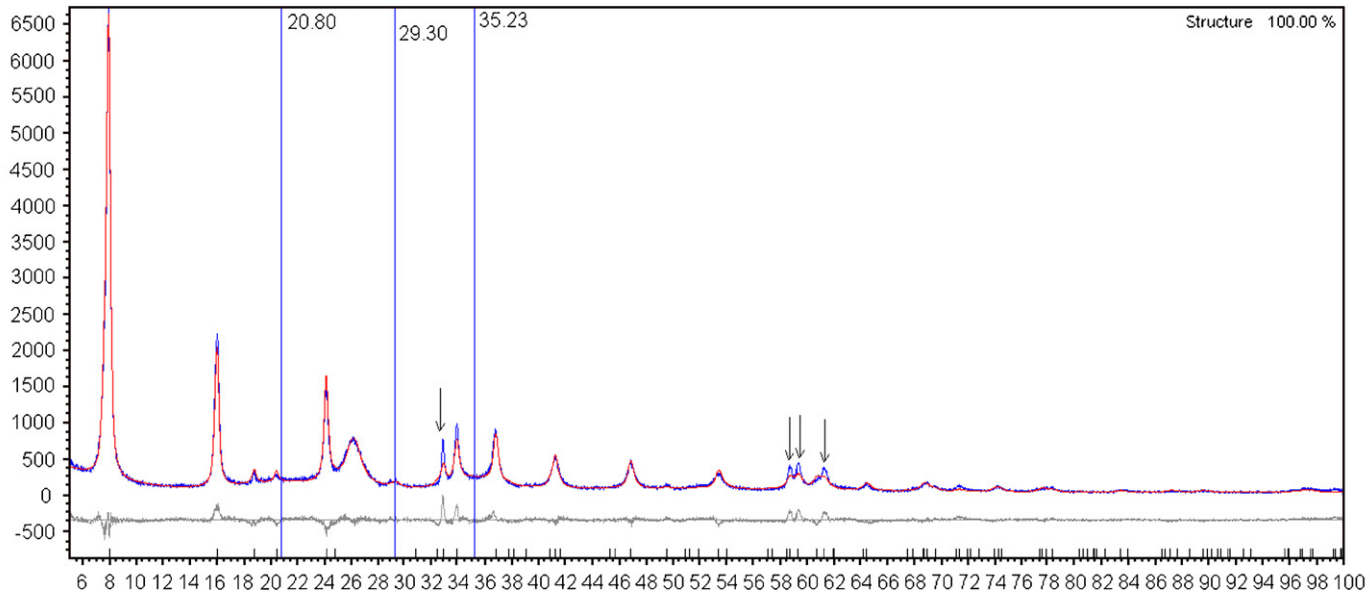

Fig. 6. Rietveld refinement plot of SO_4-LDHs. The upper curves correspond to the experimental diffraction and the calculated one. The lower curve shows the difference between calculated and experimental data.

Table 3
Positional and thermal parameters for SO_4-LDHs

Name	Site	x	y	z	Atom	Occupancy	B (nm^2)
Zn	2*c*	0.66667	0.33333	0.0	Zn	0.645	0.0088
Fe1	2*c*	0.66667	0.33333	0.0	Fe	0.355	0.0088
Fe2	1*a*	0.0	0.0	0.0	Fe	0.9131	0.0088
OH	6*k*	0.32219	0.0	0.06813		1	0.0119
S	2*e*	0.0	0.0	0.64100	S	0.349	0.0147
O_A	2*e*	0.0	0.0	0.778	O^{2-}	0.349	0.0147
O_B	6*k*	0.25600	0.0	0.59600	O^{2-}	0.349	0.0147
$O(H_2O)$	12*l*	−0.23600	0.61900	0.66300	O^{2-}	0.3686	0.08

Zn-containing GR2(SO_4^{2-}) consists of positively charged hydroxide layers $[Zn_{0.435}\cdot Fe^{II}_{0.094}\cdot Fe^{III}_{0.470}\cdot(OH)_2]^{0.470+}$ separated by about 1.104 nm; the Zn^{2+}, Fe^{2+} and Fe^{3+} cations have regular octahedral hydroxyl-coordination (see Fig. 7(a)). The negatively charged groups $[(SO_4^{2-})_{0.235}\cdot 1.0H_2O]^{0.470-}$ are alternatively close to one of the two adjacent layers, with water molecules on the opposite side. SO_4^{2-} anions are inserted in register directed by their apical atoms O of sulfate functional group towards the Fe^{3+} cations, quite similar to those in GR2(SO_4^{2-}) [6]. Fig. 7(b) presents a tentative supramolecular structural model for SO_4-LDHs.

The elemental analysis for DBS-LDHs shows the contents of Zn, Fe, S, C and H as (in wt%) 18.7%, 16.14%, 5.84%, 26.11% and 4.95%, respectively. The results confirm the Zn/Fe ratio equal to 1.00, which is quite close to the Zn/Fe input value 0.96, indicating that the coprecipitation process was rather complete. A well-defined LDH-like phase was present in the dried product and small amount of zinc ferrite was also detected in the powder XRD pattern. However, the input Fe^{2+} cations were almost completely oxidized to Fe^{3+} cations during the coprecipitation process as the chemical analysis indicated (ca. 0.43% Fe^{2+} in DBS-LDHs).

The Mössbauer spectrum of DBS-LDHs (Fig. 5(b)) displays only two asymmetrical doublets *D*3 and *D*4, which is quite similar to the room temperature MS characteristics of CO_3-containing Zn–Fe(III) [3] and Mg–Fe(III) LDHs material [33]. According to the values of δ and Δ in Table 2, iron atoms are in oxidation state of +3 in DBS-LDHs [34,35], indicating that the initially input Fe^{2+} was substantially oxidized into Fe^{3+} state during the coprecipitation process. The detectable zinc ferrite phase in precipitate probably originates from the catalytic functions of the input Fe^{2+} [35]. *D*4 with small $\Delta = 0.355$ mm/s representing 63% of the total area corresponds to randomly distributed Fe^{3+} in symmetric octahedral sites with many Zn^{2+} neighbors of the hydroxide layers [12,36,37]. *D*3 with large $\Delta = 0.731$ mm/s (37%) may correspond to Fe^{3+} in asymmetric octahedral sites with Fe^{3+} in the neighboring cation positions, indicating a comparatively strong tendency for cation segregation [3,12].

In spite of the broadening peak (Fig. 1(b)), the diffraction patterns were modeled in a first approximation by using Rietveld refining method (Fig. 8) to obtain the unit cell parameters. Since the Rietveld refining method is a full pattern analysis, the obtained lattice parameter *c* is more reliable than one derived from only the (003) reflection. In Fig. 8, we show the profile fitting result of DBS-LDHs, in which the range 1–4° was excluded. Although a single intercalated LDH phase with space group *R-3m* and lattice parameters $a = 3.05$ nm and $c = 90.00$ nm can fit the profile well, introducing an

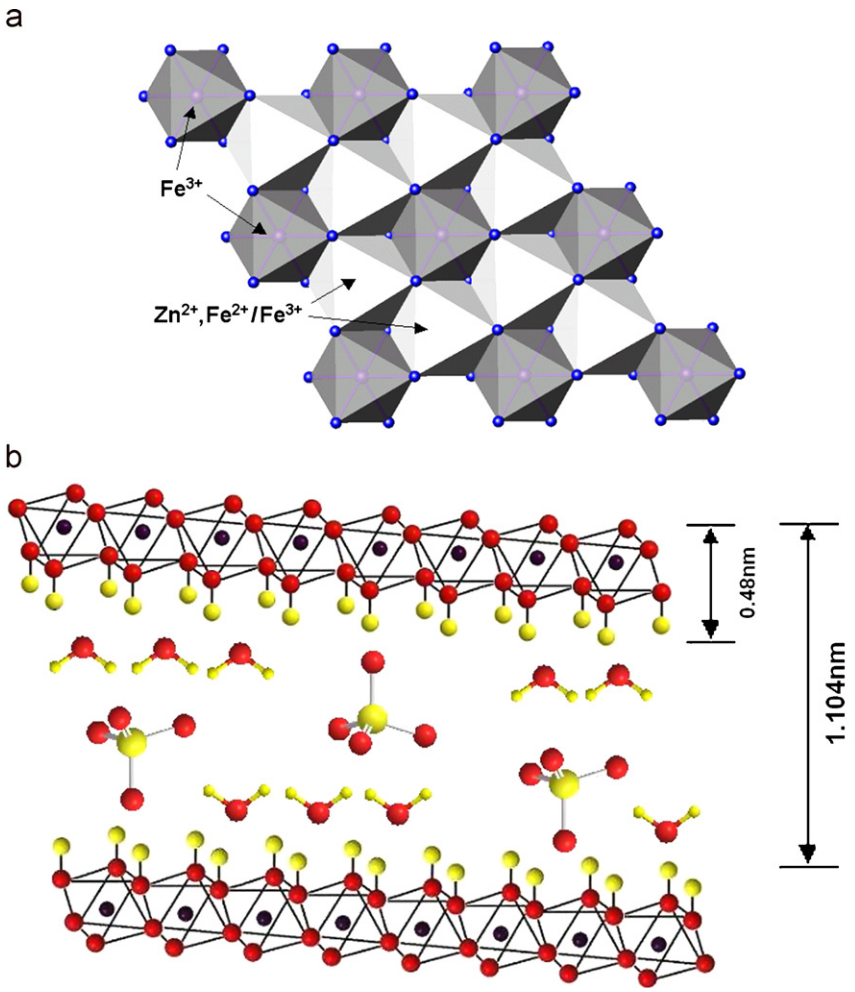

Fig. 7. The distribution of metal cation in LDH layer (a) and supramolecular structure model (b) of SO_4-LDHs.

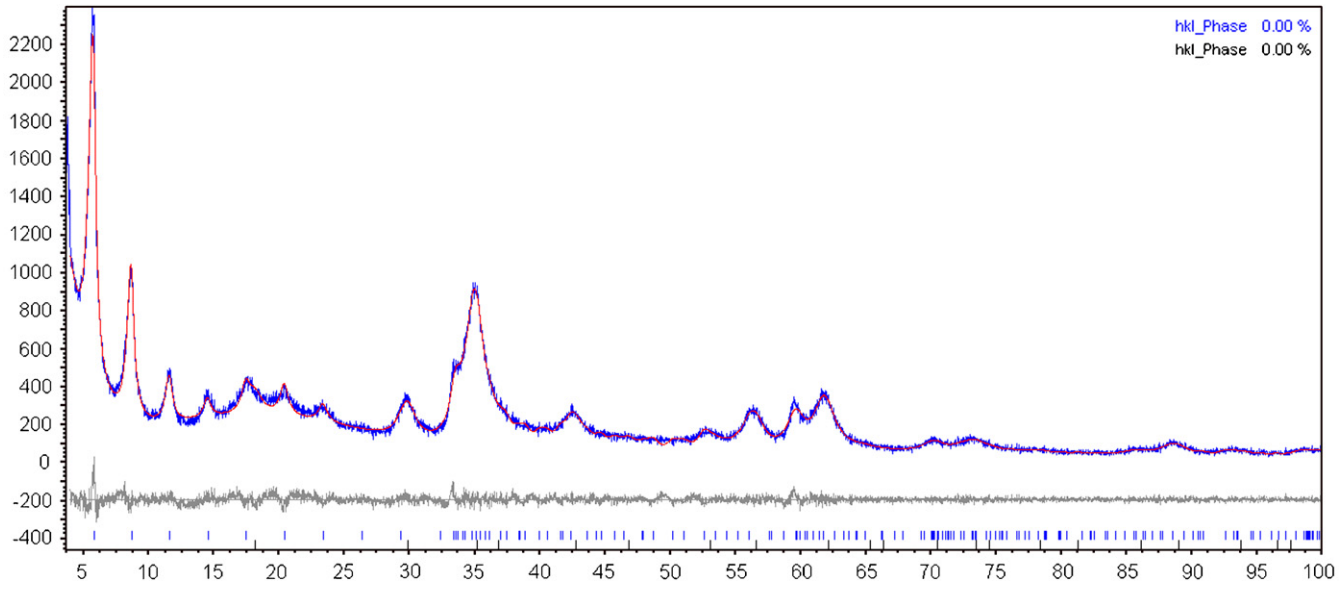

Fig. 8. The profile fitting of DBS-LDHs. The upper curves correspond to the experimental pattern and the calculated one. The lower curve shows the difference between calculated and experimental data.

additional spinel phase (zinc ferrite) ensures the refinement more reasonable, and more details and more deep explanation are still needed on this aspect.

Regarding the interactions between the benzenesulfonate group and the hydroxyl layer, some previous work should be mentioned [38–40]. Meyn et al. [38] have reported that the smaller equivalent area caused the long alkyl chain anionic surfactants to lay vertical to the LDH interlamellar surfaces, resulting in monomolecular films. Takagi et al. [39] has suggested convincingly that the actual orientation in such cases consists of two interpenetrating half-monolayers, similar to the assumption for dodecylsulfate-containing LDHs [40]. So, a three-point attachment of the sulfonate group to the LDHs layer is recommended and that the rigid phenyl ring thereby is forced to vertical to this layer. Subtracting the thickness of brucite-like layer from d_{003} value, the interlayer space of DBS-LDHs is 2.56 nm, which is larger than the molecular size of DBS along its main alkyl axis. Therefore, a possible interlayer disposition of DBS anions in prepared DBS-LDHs is probably an interpenetrating anti-parallel bilayers mode in which the alkyl chain is tilted at an angle ca. 56.9° with its long alkyl chain to the hydroxyl layer surface.

It can be clearly deduced that the intercalation of 3-dimensional anion SO_4^{2-} anion into the $ZnFe^{II}Fe^{III}$-contaning LDHs leads to the formation of Zn–$Fe^{II}Fe^{III}$ GR2-type compounds, while the intercalation of DBS anion with long alkyl chain into the $ZnFe^{II}Fe^{III}$-contaning LDHs leads to the formation of common pyroaurite-like compound DBS-Zn–Fe^{III}-LDHs.

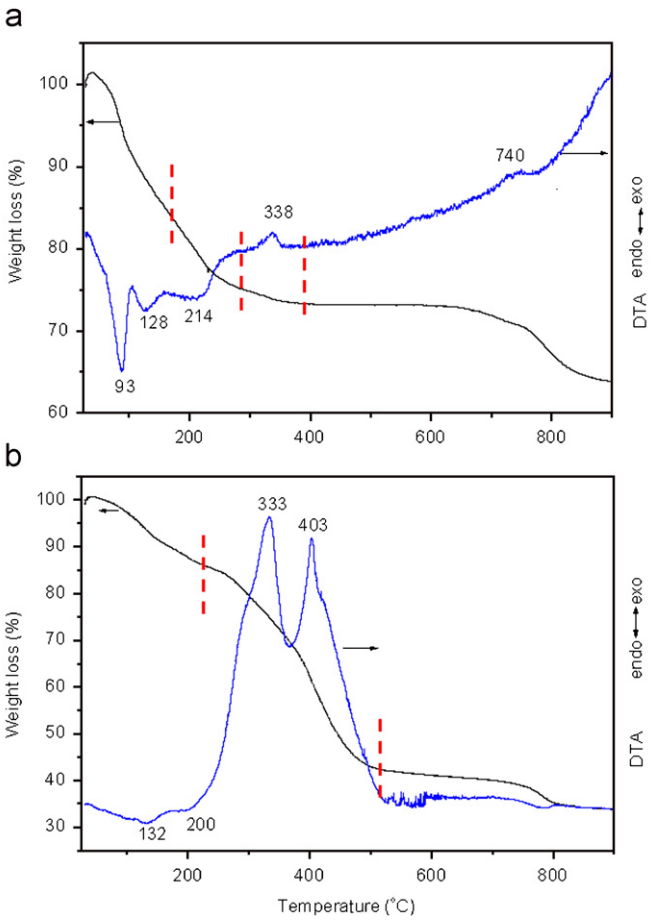

Fig. 9. TG-DTA profiles for (a) SO_4-LDHs and (b) DBS-LDHs.

3.3. Thermal characterization

In the literature, there is only one little paper on the thermal behavior of GRs-type compounds [6]. The TG-DTA curves of the SO_4-LDHs and DBS-LDHs are depicted in Fig. 9. In the case of the SO_4-LDHs (Fig. 9(a)), there are three endothermic peaks before 250 °C corresponding to departures of slightly bonded water molecules. The DTA curve shows one strong endothermic peak at 93 °C and two weak and broad endothermic ones at 128 and 214 °C, indicating that there are three-types differently bonded water molecules released during the heating process [19]. The first one is assigned to the vaporization of large amount of slightly bonded water molecules, which may characterize the even ordered interlayer structure water involving hydrogen bonding with the hydroxide layer and/or interlayer balancing SO_4^{2-} anion as FT-IR indicated. The following two endothermic peaks can mainly be attributed to the dehydroxylation of the hydroxyl groups bonded with different layer cations [6]. In particular, as bond strength of Zn–O (284 kJ/mol) much lower than that of Fe–O (409 kJ/mol), the former may be related to the Zn^{2+} cations and the latter to the Fe^{2+} and Fe^{3+} cations, where different iron cation valence give rise to asymmetric and even broadening of the endothermic peak at 214 °C. Simon et al. have reported [6] that the Fe^{2+}–Fe^{3+} GR2(SO_4^{2-}) exhibited the first strong DSC endothermic peak at 117 °C to be due to the vaporization of slightly bonded interlayer water molecules and the following one at 153 °C, due to the dehydroxylation of the hydroxide layers. It can be drawn that the present SO_4-LDHs compound exhibits slightly lower thermal stability compared to Fe^{2+}–Fe^{3+}·GR2(SO_4^{2-}) owing to the introduction of lower electronegativity Zn^{2+} cation into the LDHs layer, though they actually possess the similar interlayer disposition as indicated by XRD, FT-IR and Rietveld analyses.

The following slow mass loss event accompanying a weak exothermal peak at 338 °C is mainly due to the removal of small amount of interlayer SO_4^{2-} anions. The mass loss event at very high temperature and the corresponding weak unconnected exothermal effects at ca. 590 and 740 °C are assigned to the decomposition and combustion of SO_4^{2-} under airflow. Upon TG analysis in Fig. 9(a), it is obtained that the mass loss in the region 223–900 °C of SO_4-LDHs is ca. 17.0%, which is in good agreement with an estimated value 17.1% of SO_4^{2-} from chemical formula $[Zn_{0.435}\cdot Fe^{II}_{0.094}\cdot Fe^{III}_{0.470}\cdot(OH)_2]\cdot(SO_4^{2-})_{0.235}\cdot 1.0H_2O$.

With regard to the thermal behavior of surfactant anions-containing LDHs, Crepaldi et al. [24] reported the

thermal decomposition of DBS-intercalated Zn–Cr LDHs. In the present case of zinc–iron-containing DBS-LDHs (Fig. 9(b)), the TG curves clearly show two slow weight loss events in the temperature region 25–215 °C and a rapid one between 270 and 510 °C. The corresponding DTA plots show two weak endothermic peaks at ca. 132 and 200 °C due to the removal of interlayer structure water [2,36]. The latter endothermic peak temperature is obviously higher than that of SO_4-LDHs (128 °C), demonstrating that the limited interlayer water molecules in DBS-LDHs are mainly localized hydrogen bonding region and more strongly attached to the hydroxide layers and interlayer benzenesulfonate groups via hydrogen bonding as FT-IR indicated. More differently, a strong exothermic peak with a low-temperature shoulder at 333 °C is ascribed to the combination effect resulting from the dehydroxylation of the LDH layer, and the melt and decomposition accompanying slight combustion of the interlayer organic species DBS anions. The intimately followed remarkably strong exothermic peak around 403 °C is mainly attributed to the combustion of the intercalated DBS anions under air atmosphere [24] and trace to the continued dehydroxylation of the LDHs layer, together with the formation of mixed zinc iron oxide [1,2,24]. The mass loss between 300 and 700 °C of 58.5% for DBS-LDHs is close to the DBS content of 59.4% upon the ICP data for elemental S.

4. Conclusions

The novel Zn^{2+}-containing GR2 structure compounds sulfate-intercalated $ZnFe^{II}Fe^{III}$-LDHs and organic anion DBS-intercalated Zn–Fe LDHs materials have been synthesized by simple coprecipitation method. The MS measurement confirms the presence of both the Fe^{2+} and Fe^{3+} characteristics on the layers for SO_4-LDHs intercalate. While DBS-LDHs composite only shows the Fe^{3+} characteristics similar to the pyroaurite-type compounds, the SO_4-LDHs compound possesses chemical composition $[Zn_{0.435}Fe^{II}_{0.094}Fe^{III}_{0.470}(OH)_2]\ (SO_4^{2-})_{0.235}\cdot 1.0H_2O$. A supramolecular structure model is proposed for SO_4-LDHs based on combinational spectroscopy and Rietveld analyses. The sulfate groups alternatively close to one of two layers, interlayer water molecules dispose on the opposite side resulting in a basal spacing of 1.104 nm. For DBS-LDHs, the common pyroaurite-type structure was revealed and the DBS loading is ca. 59.4%. TG/DTA analyses indicate that the SO_4^{2-}-intercalated $Zn–Fe^{II}Fe^{III}$ compound possesses slightly lower thermal stability than typical GR2(SO_4^{2-}) compound. The contact angle measurement demonstrates the remarkable hydrophobic property of the DBS-intercalated zinc–iron LDHs composite. Comparative investigations on the adsorption behavior of as-synthesized materials aimed at environmental organic pollutants remedies are in progress in our Laboratory.

Acknowledgment

This work was supported by the National Nature Science Foundation of China (Grant No. Key 20531010) and the National Natural Science Foundation Major International Joint Research Program (Project No. 20620130108).

References

[1] H.C.B. Hansen, Geochim. Cosmochim. Acta 58 (1994) 2599.
[2] H.C.B. Hansen, C.B. Koch, Clay Minerals 33 (1998) 87.
[3] C.B. Koch, Hyperfine Interactions 117 (1998) 131.
[4] H.C.B. Hansen, S. Guldberg, M. Erbs., C.B. Koch, Appl. Clay Sci. 18 (2001) 81.
[5] J.M.R. Genin, P. Refait, G. Bourrie, M. Abdelmoula, Fabienne Trolard, Appl. Geochem. 16 (2001) 559.
[6] L. Simon, M. Francois, P. Refait, G. Renaudin, M. Lelaurain, J.M.R. Genin, Solid State Sci. 5 (2003) 327.
[7] A. Gehin, C. Ruby, M. Abdelmoula, O. Benali, J. Ghanbaja, P. Refait, J.M.R. Genin, Solid State Sci. 4 (2002) 61.
[8] H.C.B. Hansen, C.B. Koch, H. Nancke-Krogh, O.K. Borggaard, J. Sorensen, Environ. Sci. Technol. 20 (1996) 2053.
[9] S. Loyaux-Lawniczak, P. Refait, J.-J. Ehrhardt, P. Lecomte, J.-M.R. Genin, Environ. Sci. Technol. 34 (2000) 438.
[10] P. Refait, L. Simon, J.-M.R. Genin, Environ. Sci. Technol. 34 (2000) 819.
[11] J.J. Liu, F. Li, D.G. Evans, X. Duan, Chem. Mater. 16 (2004) 1597.
[12] P. Refait, M. Abdelmoula, F. Trolard, J.-M.R. Genin, J.J. Ehrhardt, G. Bourrie, Am. Mineral. 86 (2001) 731.
[13] S.P. Newman, W. Jones, New J. Chem. 22 (1998) 105.
[14] B. Wang, H. Zhang, D.G. Evans, X. Duan, Mater. Chem. Phys. 92 (2005) 190.
[15] F. Li, X. Duan, Struct. Bond. 119 (2006) 193.
[16] Y.W. You, H.T. Zhao, G.F. Vance, J. Mater. Chem. 12 (2002) 907.
[17] P.C. Pavan, E.L. Crepaldi, G. de A. Gomes, J.B. Valim, Colloids Surf. A 154 (1999) 399.
[18] P.C. Pavan, E.L. Crepaldi, J.B. Valim, J. Colloid Interface Sci. 229 (2000) 346.
[19] F. Cavani, F. Trifirò, A. Vaccari, Catal. Today 11 (1991) 173.
[20] TOPAS V2.1: General profile and structure analysis software for powder diffraction data, Bruker AXS, Karlsruhe (Germany).
[21] G.D. Christian, Analytical Chemistry, third ed, Wiley, New York, 1980.
[22] J.D. Bernal, D.R. Dasgupta, A.L. Mackay, Clay Miner. Bull. 4 (1959) 15.
[23] R. Trujillano, M.J. Holgado, J.L. González, V. Rives, Solid State Sci 7 (2005) 931.
[24] E.L. Crepaldi, P.C. Pavan, J. Tronto, J.B. Valim, J. Colloid Interface Sci. 248 (2002) 429.
[25] K. Nakamoto, Infrared and Raman Spectra of Inorganic and Coordination Compounds, 5th ed, Wiley, New York, 1997.
[26] Z.P. Xu, P.S. Braterman, J. Mater. Chem. 13 (2003) 268.
[27] J.T. Kloprogge, H. Ruan, R.L. Frost, J. Mater. Sci. 36 (3) (2001) 603.
[28] A.S. Bookin, V.A. Drits, Clays Clay Miner. 41 (1993) 551.
[29] M. Khaldi, A. De Roy, M. Chaouch, J.P. Besse, J. Solid State Chem. 130 (1997) 66.
[30] Y.W. You, H.T. Zhao, G.F. Vance, Colloids Surf. A 205 (2002) 161.
[31] H. Chen, F. Zhang, S. Fu, X. Duan, Adv. Mater. 18 (2006) 3089.
[32] E.M. Moujahid, J.P. Besse, F. Leroux, J. Mater. Chem. 13 (2003) 258.
[33] P.S. Kumbhar, J. Sanchez-Valente, J.M.M. Millet, F. Figueras, J. Catal. 191 (2000) 467.
[34] J. W. Niemantsverdriet, Spectroscopy in catalysis, VCH Verlagsgescllschaft mbH, D-69451 Weinheim, New York, 1993, pp. 111.

[35] H. Liu, Y. Wei, Y. Sun, J. Mol. Catal. A 226 (2005) 135.
[36] C.N. Chinnasamy, A. Narayanasamy, N. Ponpandian, K. Chattopadhyay, Mater. Sci. Eng. A 304–306 (2001) 983.
[37] J.M.R. Genin, M. Abdelmoula, P. Refait, L. Simon, Hyperfine Interact. C 3 (1998) 313.
[38] M. Meyn, K. Beneke, G. Lagaly, Inorg. Chem. 29 (1990) 5201.
[39] K. Takagi, T. Shichi, H. Usami, Y. Sawaki, J. Am. Chem. Soc. 115 (1993) 4339.
[40] A. Clearfield, M. Kieke, J. Kwan, J.L. Colon, R.C. Wang, J. Inclusion Phenom. Mol. Recognit. Chem. 11 (1991) 361.